RSC Advances

PAPER

View Article Online
View Journal | View Issue

Check for updates

Cite this: *RSC Adv.*, 2023, **13**, 3459

Liposomes loaded with dual clinical photosensitizers for enhanced photodynamic therapy of cervical cancer

Gulinigaer Alimu,[a] Ting Yan,[a] Lijun Zhu,[b] Zhong Du,[c] Rong Ma,[c] Huimin Fan,[b] Shuang Chen,[c] Nuernisha Alifu *[ab] and Xueliang Zhang*[ab]

Photodynamic therapy (PDT) has become a potential anti-cancer strategy owing to its negligible invasiveness, low toxicity, and high selectivity. The photosensitizer (PS) plays an indispensable role in PDT. Herein, a novel type of PS (Ce6-MB@Lips) which can be excited by a near-infrared (NIR) laser was designed and synthesized. Methylene blue (MB) and Chlorin e6 (Ce6), two organic dyes approved by the Food and Drug Administration (FDA), were used to prepare Ce6-MB@Lips by thin-film dispersion method, which improve the water solubility of Ce6 and reduce the cytotoxicity of MB. The Ce6-MB@Lips were shown to have a spherical nanostructure with an average particle size of 160.3 nm and excellent water solubility. Then the optical properties of Ce6-MB@Lips were further studied. Ce6-MB@Lips showed absorption peaks at 413 nm/670 nm and fluorescence peak at 697 nm. Compared with Ce6@Lips and MB@Lips, Ce6-MB@Lips showed better stability, stronger fluorescence intensity, and higher singlet oxygen ($^1O_2$) generation ability. Cell experimental analysis exhibited that the stable Ce6-MB@Lips showed low cytotoxicity, high phototoxicity and high reactive oxygen species (ROS) production capacity. After effective cell internalization, the prepared Ce6-MB@Lips showed excellent ability to promote tumor cell apoptosis *in vitro*. The Ce6-MB@Lips could be a promising candidate for PDT of cervical cancer.

Received 14th May 2022
Accepted 13th January 2023

DOI: 10.1039/d2ra03055a

rsc.li/rsc-advances

Open Access Article. Published on 24 January 2023. Downloaded on 2/25/2026 2:49:08 PM.
This article is licensed under a Creative Commons Attribution-NonCommercial 3.0 Unported Licence.

Introduction

Cancer is one of the leading causes of death worldwide, and cervical cancer is the fourth most common malignancy diagnosed in women.[1,2] In recent years, the incidence rate of cervical cancer has been high at a young age.[3,4] It is a devastating disease that results from an uncontrollable growth of tumor cells and their subsequent spread across the body. At present, various methods have been used for the diagnosis and screening of cervical cancer. For example, pap smear cytology and DNA testing are performed in cases of human papillomavirus (HPV) infection.[5,6] The treatment of cervical cancer includes surgical treatment, external irradiation radiotherapy, brachytherapy, and concurrent cisplatin chemotherapy.[1,7] However, drug tolerance, non-specificity, and unavoidable side effects hinder their further development.[8–10] As an alternative emerging treatment, photodynamic therapy (PDT) brings a new dawn.[11]

PDT has emerged as an effective therapeutic alternative for tumor treatment. The PDT process includes three key components—a photosensitizer (PS), a light source of the ideal wavelength, and reactive oxygen species (ROS).[12–14] When the PS is irradiated by a laser of a specific wavelength, it can transfer energy to oxygen or oxygen-containing groups in the surrounding environment, and finally generates ROS.[15–19] PDT exhibited superiority such as minimal invasiveness, favourable safety, fewer side effects, good repeatability, and relatively low cost. It plays an important role in the comprehensive treatment of tumors.[20–23] However, the clinical application of PDT is still limited by the depth of tissue penetration.[24] Therefore, we utilized the laser in the near-infrared I (NIR-I) spectral region (650–950 nm)[25–27] as excitation light in order to reduce tissue autofluorescence and scattering from the biological tissue, which could help to penetrate into deep tumor.

In recent years, the NIR-I light are favorable as the excitation light for PDT, for longer wavelength and deep tissue penetration ability. Among various PSs, Chlorin e6 (Ce6), an FDA-approved second-generation PS with absorption peaks around 407 nm and 660 nm,[28] is extensively used in PDT because of its lipophilic characteristics[29] and high singlet oxygen ($^1O_2$) generation efficiency.[30] However, the poor water solubility of Ce6 leads to

[a]*Department of Epidemiology and Health Statistics, School of Public Health, Xinjiang Medical University, Urumqi, 830054, China. E-mail: shuxue2456@126.com; nens_xjmu@126.com*

[b]*State Key Laboratory of Pathogenesis, Prevention and Treatment of High Incidence Diseases in Central Asia, School of Medical Engineering and Technology, Xinjiang Medical University, Urumqi, 830054, China*

[c]*Department of Gynecology, The First Affiliated Hospital of Xinjiang Medical University, Urumqi, 830054, China*

© 2023 The Author(s). Published by the Royal Society of Chemistry

Open Access Article. Published on 24 January 2023. Downloaded on 2/25/2026 2:49:08 PM. This article is licensed under a Creative Commons Attribution-NonCommercial 3.0 Unported Licence.

low PDT efficacy and hinders their further biomedical applications.[31–33] Methylene blue (MB) is another FDA-approved hydrophilic second-generation PS,[34] with absorption peak around 664 nm.[35,36] Thus, as the NIR dyes,[37,38] under NIR-I irradiation, Ce6 and MB have well PDT property for the deep penetration ability of excitation light. Especially, the usage of a single wavelength laser could bring great convenience.

Liposomes are one of the ideal drug carriers with the construction of amphiphilic phospholipid bilayers.[39] The morphology of liposomes is similar to cellular membranes. Therefore, liposomes obtains excellent biocompatibility which could incorporate various substances.[40] In cancer therapy, liposomes have been demonstrated to be particularly useful.[41] Liposomes can increase the hydrophilicity of PS and enhance the ability of PS engulfed by tumor cells.[42] Liposomes have been introduced into more fields, including the development of novel agents for PDT.[43] Zhang *et al.* prepared a liposome loaded with PS Ce6, hypoxia-activated prodrug Tirapazamine (TPZ), and a gene probe for synergistic photodynamic chemotherapy.[44]

Herein, to improve water solubility and achieve highly efficient photodynamic efficacy, we designed and synthesized a new type of PS (Ce6-MB@Lips) by the film dispersion method. We used two FDA-approved organic dyes MB and Ce6 to prepare low-toxicity and effective nanoplatforms, which can achieve high-efficiency photodynamic effects under the guidance of NIR fluorescence imaging. Ce6-MB@Lips showed absorption peaks at 413 nm and 670 nm and fluorescence peak at 697 nm. Compared with Ce6@Lips and MB@Lips, Ce6-MB@Lips had better optical properties and stability. Through cell experiments, we tested the biological activity of Ce6-MB@Lips on HeLa and SiHa cells, including phototoxicity, dark toxicity, cellular uptake, and apoptosis rate. And it was proved that Ce6-MB@Lips had a good ability to produce ROS (O_2) under a 660 nm laser irradiation, which was verified by 9,10-anthracenediyl-bis (methylene) dimalonic acid (ABDA) and 2,7-dichlorodi-hydrofluorescein diacetate (DCFH-DA) probes *in vitro*. And the PDT therapeutic efficiency of Ce6-MB@Lips applied to HeLa cells was 78.35%; the PDT therapeutic efficiency applied to SiHa cells was 68.45%. This means Ce6-MB@Lips is a promising PS for the PDT treatment of cervical cancer.

Experimental section

Materials and instruments

The L-α-phosphatidylcholine and cholesterol were obtained from Beijing Solarbio Science & Technology Co., Ltd in China. Chlorin e6 (Ce6) and 9,10-anthracenediyl-bis (methylene) dimalonic acid (ABDA) were purchased from Shanghai Macklin Biochemical Co., Ltd. Methylene blue (MB) was purchased from Shanghai Aladdin Biochemical Technology Co., Ltd. Methylidyne trichloride ($CHCl_3$) and tetrahydrofuran (THF) were procured from the Central-Lab of the Medical University in Xinjiang. Hoechst 33342 and enhanced cell counting kit-8 (CCK8) were obtained from Beijing Solarbio Science & Technology Co., Ltd in China. And 2,7-dichlorodi-hydrofluorescein diacetate (DCFH-DA) was purchased from Beyotime Biotechnology in China. Dulbecco's modified essential medium (DMEM), phosphate buffered saline (PBS), and fetal bovine serum (FBS) were purchased from GIBCO, and deionized water (DIW) was used in all experimental process.

The morphology and size of liposomes were measured by transmission electron microscope (TEM, JEM-1230, Japan). The particle size distribution was measured by dynamic light scatting analysis (DLS, Malvern, UK). The absorbance spectra and fluorescence spectra were recorded from a Shimadzu UV-2700 UV-Vis spectrophotometer (Japan) and Shimadzu RF-5301PC spectrofluorophotometer (Japan). A confocal laser scanning microscope (CLSM, NIKON C2+, Japan) was utilized for the NIR fluorescence microscopic imaging. A flow cytometer (BD, LSR II, America) was used to detect the apoptosis rate and the production of ROS.

Synthesis of Ce6-MB@Lips

Ce6-MB@Lips was synthesized by the thin-film dispersion method. 40 mg of lecithin, 10 mg of cholesterol, and 4 mg of Ce6 were weighed with an electronic balance and dissolved in appropriate amounts ($CHCl_3$/THF = 1 : 1, v/v) to form a mixed solution. Then the film was formed by rotating evaporation on a magnetic stirrer, and MB solution (the solvent was DIW and PBS) was added. Next, the mixture was placed in a 40 °C water bath for ultrasonic mixing for 30 min. Then the solution was placed in a dialysis bag for 24 h to separate free Ce6 and MB and then filtered by a 0.22 μm microporous membrane to obtain co-encapsulated MB and Ce6 liposomes suspension (Ce6-MB@Lips). Blank liposomes, single-coated liposomes containing MB (MB@Lips), and single-coated liposomes containing Ce6 (Ce6@Lips) were prepared by the same method. The resulting nanoparticles were stored at 4 °C for future use.

Characterization

The absorption spectra of free Ce6 and MB, Ce6@Lips, MB@Lips, and Ce6-MB@Lips solutions (5 μg mL^{-1}) were measured by a Shimadzu UV-2700 UV-Vis spectrophotometer, and the absorption values were measured for five consecutive days to observe its stability. The fluorescence spectra of Ce6, MB, Ce6@Lips, MB@Lips, and Ce6-MB@Lips solutions (100 μg mL^{-1}) were determined using an RF-5301PC spectrofluorophotometer. The morphology and particle size of Ce6@Lips, MB@Lips and Ce6-MB@Lips were observed by transmission electron microscopy (TEM) and dynamic laser light scatterometer (DLS). The fluorescence intensity of Ce6, MB, Ce6@Lips, MB@Lips, and Ce6-MB@Lips solutions was observed by confocal microscopy (CLSM).

Release rate, drug loading and entrapment efficiency

The release rate of PS is an important indicator. Thus, we used the UV-2700 Shimadzu ultraviolet spectrograph to calculate the cumulative release of PSs from Ce6-MB@Lips at pH values of 7.4, 5.4 and 5 *in vitro*.[45] To do this, the Ce6-MB@Lips (15 mL, 30 μg mL^{-1}) in the solution were stirred with a magnetic stirrer at 37 °C and 1000 rpm. At different times (0, 2, 4, 6, 8, 10, 12, 24, 36 and 48 h), we removed 2 mL of this Ce6-MB@Lips and added

© 2023 The Author(s). Published by the Royal Society of Chemistry

Open Access Article. Published on 24 January 2023. Downloaded on 2/25/2026 2:49:08 PM. This article is licensed under a Creative Commons Attribution-NonCommercial 3.0 Unported Licence.

2 mL of fresh pH solution. The cumulative release rates of PSs in Ce6-MB@Lips were calculated at 665 nm. To determine drug loading content (DLC) and encapsulation efficiency (EE), supernatants from three centrifugation cycles were collected when preparing Ce6-MB@Lips. We measured the absorption spectrum of Ce6 and MB using the UV-2700 ultraviolet spectrograph at 665 nm. The concentrations of Ce6 and MB in Ce6-MB@Lips were acquired using the standard curve method and calculated by using the following formulas:[46,47]

$$\text{DLC}\ (\%) = \frac{W_{\text{Ce6/MB}} - W_{\text{drug in supernatant}}}{W_{\text{Ce6-MB@Lips}}} \quad (1)$$

$$\text{EE}\ (\%) = \frac{W_{\text{Ce6/MB}} - W_{\text{drug in supernatant}}}{W_{\text{T}}} \quad (2)$$

where the $W_{\text{Ce6/MB}}$ is the quantity of Ce6 or MB in the Ce6-MB@Lips, $W_{\text{Ce6-MB@Lips}}$ is the weight of the Ce6-MB@Lips, and W_{T} was the total weight of the Ce6 or MB added.

Singlet oxygen detection

Singlet oxygen ($^1O_2$) is one of the important indexes for the efficacy of PDT.[48] It has high oxidation activity and ROS to change the spectrum of the detection agent. We selected the $^1O_2$ detector ABDA.[49] Under the 660 nm laser irradiation, ABDA can irreversibly react with the $^1O_2$ produced by the PS, resulting in a decrease in ABDA fluorescence intensity. ABDA solution (100 μL, 1 mg mL^{-1} in DMSO) was added into Ce6, MB, Ce6@Lips, MB@Lips and Ce6-MB@Lips solutions (10 μg mL^{-1}) respectively. The mixture was then irradiated with a laser (660 nm, 1 W cm^{-2}) and the absorption spectra of the mixture were measured every 15 s for 120 s.

Cell culture

Human cervical cancer cells (SiHa and HeLa) and cervical normal cells (H8) were obtained from the American Type Culture Collection (ATCC), and these cells were routinely maintained in DMEM containing 1% penicillin/streptomycin and 10% FBS.[50] And the incubation environment was maintained at 37 °C and with 5% CO_2.

In vitro cytotoxicity and phototoxicity assay

H8 and HeLa cells (5×10^3 cells per well) at the logarithmic growth stage were inoculated into 96-well plates and incubated for 24 h at 37 °C. Then the culture medium was replaced with 100 μL of culture medium containing Ce6@Lips, MB@Lips, and Ce6-MB@Lips (10, 20, 40, 60, 80, 100 μg mL^{-1}) and incubated for 6 h, then CCK8 (10 μL) was added and incubated for 2 h and the OD values were measured by a Thermo Scientific Multiskan FC and the cell viability and 50% inhibiting concentration (IC50) were calculated. To evaluate phototoxicity, the cells were treated with Ce6-MB@Lips under the same conditions but with laser exposure (660 nm, 1 W cm^{-2}, 5 min). The cell viability was calculated using the following formula:[51]

$$\text{Cell viability}\ (\%) = \frac{\text{OD}_\text{E} - \text{OD}_\text{B}}{\text{OD}_\text{C} - \text{OD}_\text{B}} \times 100\% \quad (3)$$

In this formula, OD_E is the average value of absorbance in the trial group, OD_B is the average value of absorbance in the blank group, and OD_C is the average value of absorbance in the control group.

Cellular uptake

A fluorescence imaging method was used to evaluate Ce6-MB@Lips, which was analyzed by a CLSM to determine whether it has a great ability to label cells, and compared with Ce6, MB, Ce6@Lips and MB@Lips. HeLa cells in the logarithmic growth phase were inoculated in confocal dishes with 2.5×10^5 cells (500 μL) and placed overnight in an incubator (5% CO_2, 37 °C). Then the cells were washed with 1× PBS three times, and 500 μL complete media containing free Ce6 or MB (15 μg mL^{-1}), and Ce6@Lips, MB@Lips and Ce6-MB@Lips (20 μg mL^{-1}) were added to the HeLa cells for 2 h, and the supernatant was discarded and washed three times with 1× PBS, followed by the addition of 500 μL of Hoechst 33342 dye liquor (1 : 100) reacting for 20 min. Then cells were washed with 1× PBS three times, and 500 μL of fresh complete culture solution was added to each dish. CLSM fluorescence imaging was performed.

Cellular ROS generation detection

The production of ROS intracellular was determined *via* the DCFH-DA probe which had no fluorescence and could pass through the cell membrane freely with 660 nm laser irradiation. To better verify the experimental phenomenon, HeLa and SiHa cells were selected to be seeded in confocal dishes and cultured for 24 h at 37 °C, followed by treatment with Ce6, MB, Ce6@Lips, MB@Lips and Ce6-MB@Lips at the concentration of 20 μg mL^{-1} for 2 h. Then the cells were washed with 1× PBS three times and stained with Hoechst 33342 dye liquor (1 : 100) for 20 min and DCFH-DA (5 μM, 500 μL) for 30 min. Then the cells were washed with 1× PBS again, after that, they were irradiated for 5 min (660 nm, 1 W cm^{-2}), and the generation of ROS was observed by CLSM.[52,53]

The amount of ROS produced in HeLa and SiHa cells was quantitatively assessed by a flow cytometer to verify the PDT efficacy of Ce6-MB@Lips. HeLa and SiHa cells (2×10^5 cells per well) were inoculated in 6-well plates and incubated at 37 °C for 24 h, then the cells were washed with PBS and Ce6-MB@Lips (20 μg mL^{-1}) were added. After incubation for 2 h, the cells were washed twice with PBS and treated with 10 μM DCFH-DA for 30 min at 37 °C. Then, the cells were irradiated with a 660 nm laser (1 W cm^{-2}) for 5 min, and the intracellular ROS concentration was quantitatively determined by a flow cytometer.

Apoptotic analysis

PDT-induced apoptosis and necrosis were detected using the Annexin-V-FITC/PI apoptosis detection kit. HeLa and SiHa cells were plated in 6-well plates (2×10^5, 2 mL) and incubated overnight. Subsequently, the cells were treated with a medium containing free Ce6, MB, Ce6@Lips, MB@Lips, and Ce6-MB@Lips at an equivalent concentration of 20 μg mL^{-1}. After 2 h, the cells were washed with PBS and then irradiated with a 660 nm laser for 5 min. Afterward, cells were harvested and

Open Access Article. Published on 24 January 2023. Downloaded on 2/25/2026 2:49:08 PM.
This article is licensed under a Creative Commons Attribution-NonCommercial 3.0 Unported Licence.

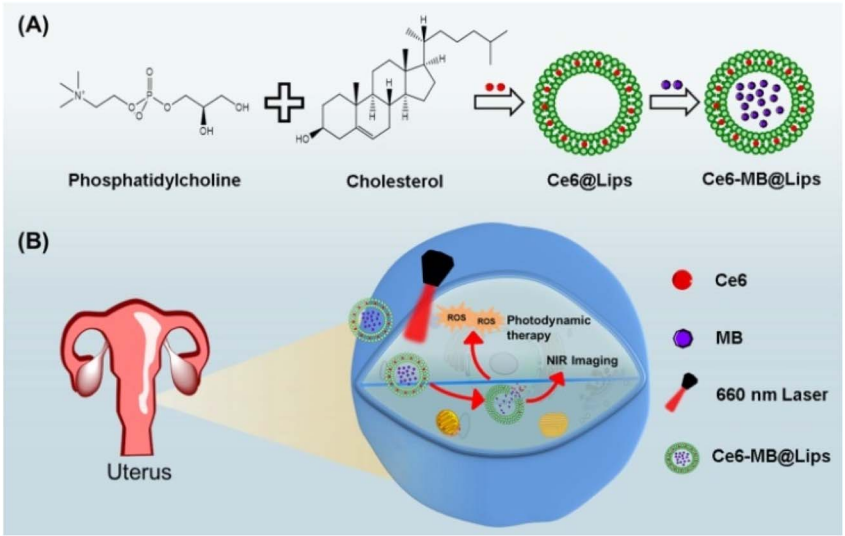

Scheme 1 (A) Ce6-MB@Lips preparation process description. (B) Schematic diagram of the role of Ce6-MB@Lips in tumor cells.

suspended in a binding buffer. Finally, the samples were stained with Annexin-V-FITC (5 μL) and PI (5 μL) for 10 min in the dark and then analyzed by a flow cytometer.

Results and discussion

Synthesis and characterization of Ce6-MB@Lips

The synthesis process of Ce6-MB@Lips is shown in the Scheme 1, Ce6 was first coated with liposomes to form a suspension (Ce6@Lips), and MB was further loaded to form a murky dark green solution (Ce6-MB@Lips), as shown in Fig. 1A. The TEM images (Fig. 1B) showed the spherical nanostructure of Ce6-MB@Lips, and the average particle size was 113.4 nm. The average diameter of Ce6-MB@Lips was further determined by DLS as 160.3 nm (Fig. 1C). The UV-Vis spectra (Fig. 1D) showed that Ce6 has two absorption peaks at 404 nm and 660 nm, and MB has a maximum absorption peak at 664.5 nm. Ce6-MB@Lips owned peak absorption wavelength at

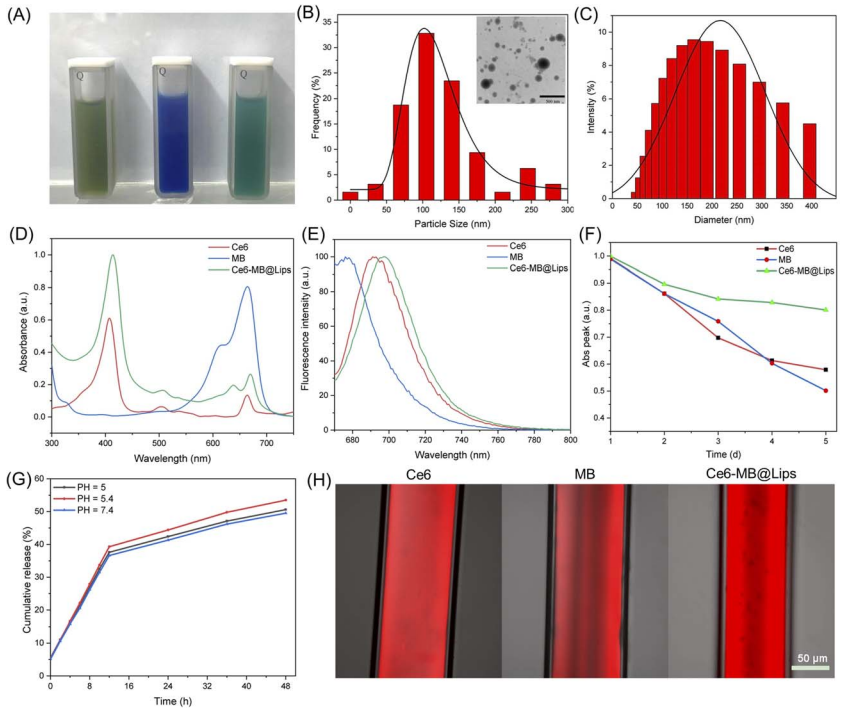

Fig. 1 Characterization of Ce6-MB@Lips. (A) Picture of Ce6@Lips, MB@Lips and Ce6-MB@Lips. (B) TEM image of Ce6-MB@Lips and corresponding histogram of particle size. (C) The size distribution of Ce6-MB@Lips was measured by DLS. (D) UV-Vis spectra of Ce6, MB, and Ce6-MB@Lips. (E) Fluorescence spectra of Ce6, MB, and Ce6-MB@Lips. (F) Changes in the absorption of Ce6, MB, and Ce6-MB@Lips for five consecutive days. (G) The release rate of PS. (H) Fluorescence images of Ce6, MB, and Ce6-MB@Lips in a capillary glass tube under a CLSM (λ_{ex} = 640 nm, λ_{em} = 800–1000 nm).

© 2023 The Author(s). Published by the Royal Society of Chemistry

Open Access Article. Published on 24 January 2023. Downloaded on 2/25/2026 2:49:08 PM. This article is licensed under a Creative Commons Attribution-NonCommercial 3.0 Unported Licence.

413 nm and 670 nm overlapping with that of Ce6 and MB. The optical characterization indicated that the encapsulation of liposomes did not change the characteristics of free Ce6 and MB. The fluorescence spectra (Fig. 1E) suggested that Ce6-MB@Lips also has luminescent properties, and even the fluorescence intensity is stronger than that of free Ce6 and MB, this was also demonstrated by capillary glass tube diagrams (Fig. 1H). As shown in Fig. 1F, Ce6-MB@Lips and the maximum absorption peak decreased by less than 20% on the fifth day compared to the first day, while the absorption values of Ce6 and MB solutions decreased significantly, proving that Ce6-MB@Lips were more stable than free Ce6 and MB.

Release rate, drug loading and entrapment efficiency

As a significant index, the release rate of PS was studied. We simulated the PS release behavior of Ce6-MB@Lips at 37 °C by using neutral conditions (pH = 7.4), an acidic microenvironment of cancer cells (pH = 5.4) and a lysosomal environment (pH = 5).[53,54] As shown in Fig. 1G, pH value significantly affected the release rate of PS in Ce6-MB@Lips. In 6 h, at pH = 7.4, the Ce6-MB@Lips released 20.6% of PS, while at pH = 5 and 5.4, 21.3% and 22.1% were released, respectively. At pH = 7.4, 49.5% of PS was released from Ce6-MB@Lips within 48 h, while 50.6% and 53.4% were released at pH = 5 and 5.4, respectively. These results indicated that the release rate in the simulated microenvironment of cancer cells is higher than that in the neutral environment.

As an excellent delivery system, liposomes can help to increase the hydrophobicity of PSs and enhance the absorption of PSs by the tumor. Free Ce6 and MB were successfully encapsulated in liposomes; we calculated the DL and EE of Ce6 and MB in Ce6-MB@Lips by UV-2700 spectroscopy. The EE of Ce6 and MB was 84.3% and 45.3% respectively, and the DLC of Ce6 and MB was 8.1% and 2.9% respectively.

Detection of singlet oxygen production

ABDA probes were used to assess the extent of $^1O_2$ production after 660 nm laser irradiation.[55] Under the same experimental conditions, the relative absorbance of ABDA at 378 nm in a solution containing Ce6 only decreased to 72.9% of its original value while Ce6@Lips decreased to 65.2% (Fig. 2A and D). And the relative absorbance of ABDA at 378 nm in MB solution decreased to 82.1% while the MB@Lips decreased to 90.6% (Fig. 2B and E). These results showed that the coating of liposomes did improve the $^1O_2$ production ability of Ce6 and MB. As illustrated in Fig. 2E, in the presence of Ce6-MB@Lips and after 120 s of 660 nm laser stimulation, the absorbance of ABDA at 378 nm decreased to 9.4% of its original value.[56,57] However, the Ce6-MB@Lips group without laser exposure decreased by only 2.5%, which was negligible (Fig. 2C). These results confirmed that Ce6-MB@Lips had an excellent ability to produce $^1O_2$ when exposed to a 660 nm laser, and the PS could produce $^1O_2$ for PDT only when the laser exists.

In vitro cytotoxicity and phototoxicity

After laser irradiation at the appropriate wavelength, the PS is triggered to produce $^1O_2$ for treatment. However, it should not show great cytotoxicity in the absence of a laser. To compare the cytotoxicity of Ce6@Lips, MB@Lips, and Ce6-MB@Lips *in vitro*, we evaluated the effect of cell viability with/without laser irradiation by the CCK8 method.

As shown in Fig. 3A and B, Ce6@Lips, MB@Lips and Ce6-MB@Lips at concentrations ranging from 10 μg mL^{-1} to 100 μg mL^{-1} was co-cultured with HeLa/H8 cells for 6 h. The IC50 of Ce6@Lips, MB@Lips and Ce6-MB@Lips in HeLa cells were 71.12 μg mL^{-1}, 53.30 μg mL^{-1} and 109.98 μg mL^{-1} while the IC50 in H8 cells were 77.45 μg mL^{-1}, 66.25 μg mL^{-1} and 138.81 μg mL^{-1}. These results indicated that Ce6@Lips, MB@Lips and Ce6-MB@Lips had lower cytotoxicity to normal cells, and the

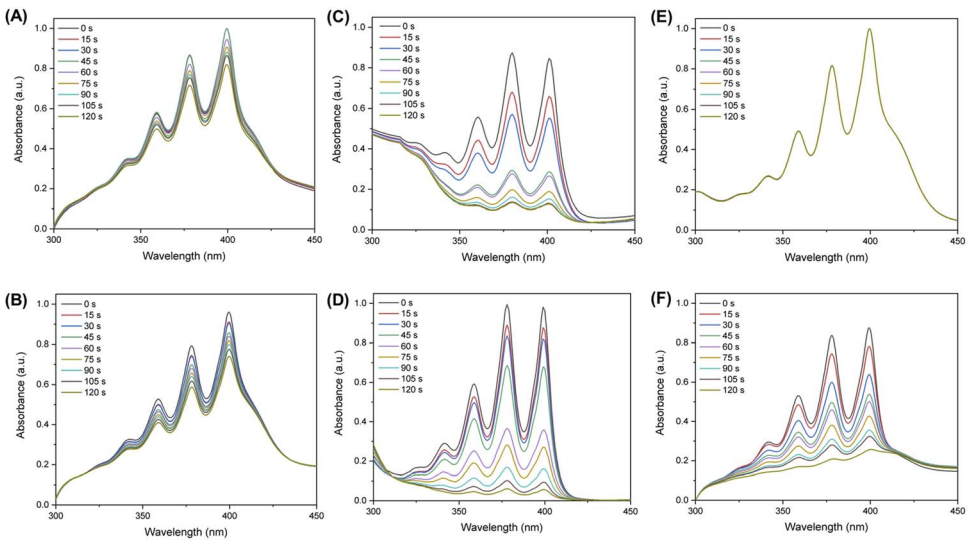

Fig. 2 Detection of $^1O_2$ production. (A) Ce6, (B) Ce6@Lips, (C) MB, (D) MB@Lips and (E) Ce6-MB@Lips under the 660 nm laser (1 W cm^{-2}) generates $^1O_2$, and then $^1O_2$ reacted with ABDA. (F) Ce6-MB@Lips without laser irradiation. Finally, the OD values of ABDA were measured. All OD values were normalized at the beginning of irradiation.

Open Access Article. Published on 24 January 2023. Downloaded on 2/25/2026 2:49:08 PM. This article is licensed under a Creative Commons Attribution-NonCommercial 3.0 Unported Licence.

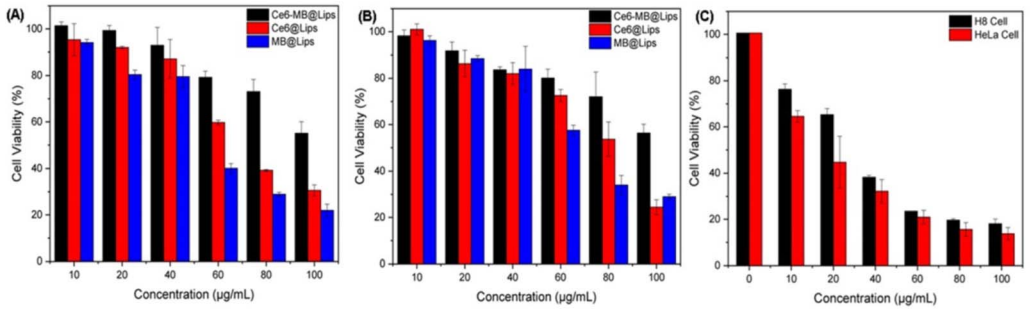

Fig. 3 Cell viability analysis of (A) HeLa cells incubated with dark, (B) H8 cells incubated with dark, and (C) HeLa and H8 cells incubated with Ce6-MB@Lips with the laser (660 nm, 1 W cm^{-2}, 5 min).

dark toxicity of Ce6-MB@Lips to cells was lower than that of Ce6@Lips and MB@Lips.

As shown in Fig. 3C, only laser irradiation did not reduce the cell viability, indicating that laser alone would not damage cells. At the same concentration, the Ce6-MB@Lips treated group showed high cell viability, indicating that its dark toxicity to HeLa and H8 cells was low. Then, after laser irradiation, the cell viability significantly decreased with the increase in concentration. However, the viability of HeLa cells decreased more obviously than that of H8 cells. Ce6-MB@Lips even at 10 μg mL^{-1} also had strong phototoxicity to HeLa cells, which could reduce the cell survival rate to 64.6%. When the concentration reached 100 μg mL^{-1}, the cell viability decreased to 13.7%. The results showed that Ce6-MB@Lips had strong phototoxicity to HeLa cells.

Cellular uptake

To determine the ability of Ce6-MB@Lips to be absorbed through cell membranes and compared with free Ce6 and MB, we studied the absorption of these PSs by HeLa cells *in vitro*. HeLa cell nuclei were stained with Hoechst 33342 which showed blue fluorescence, while the PS fluoresces red. As shown in Fig. 4, Ce6, MB, Ce6@Lips, MB@Lips and Ce6-MB@Lips could all be absorbed by the cells and were widely distributed in the cytoplasm, and the NIR fluorescence in the cytoplasm of HeLa cells incubated with of the Ce6-MB@Lips group was the strongest and the number of cells was the largest. It was turn out to be that Ce6-MB@Lips had a strong ability to enter HeLa cells and achieve NIR fluorescence imaging, locate and label HeLa cells. It may be that the improvement of water solubility enhanced the absorption of PS in HeLa cells. This result reflected that Ce6-MB@Lips was a good candidate with excellent imaging and tumor internalizing ability for NIR fluorescence imaging-guided PDT treatment.

Intracellular ROS assay

DCFH-DA was able to penetrate cells well without obvious spontaneous fluorescence.[58] And it showed significantly enhanced green fluorescence when degraded by intracellular lipase into DCF and oxidized by ROS, which provided the possibility of evaluating cell ROS generation. As shown in Fig. 5A, when there was no PS in the control group, DCFH-DA had almost no green fluorescence after laser irradiation; it showed that DCFH-DA had no spontaneous fluorescence. After laser irradiation (660 nm, 1 W cm^{-2}, 5 min), the free Ce6 group and free MB group still showed weak fluorescence, by

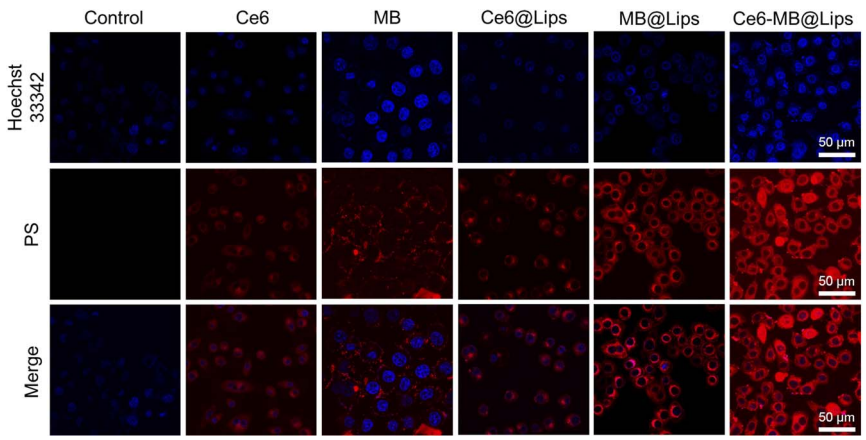

Fig. 4 Cell uptaking images after co-incubation of Ce6, MB, Ce6@Lips, MB@Lips, Ce6-MB@Lips with HeLa cells for 2 h under CLSM (scale bar: 50 μm, λ_{ex} = 640 nm, λ_{em} = 800–1000 nm). The blue fluorescence was attributed to the cell nucleus (stained by Hoechst 33342), the red fluorescence was due to the PSs.

© 2023 The Author(s). Published by the Royal Society of Chemistry

Open Access Article. Published on 24 January 2023. Downloaded on 2/25/2026 2:49:08 PM.
This article is licensed under a Creative Commons Attribution-NonCommercial 3.0 Unported Licence.

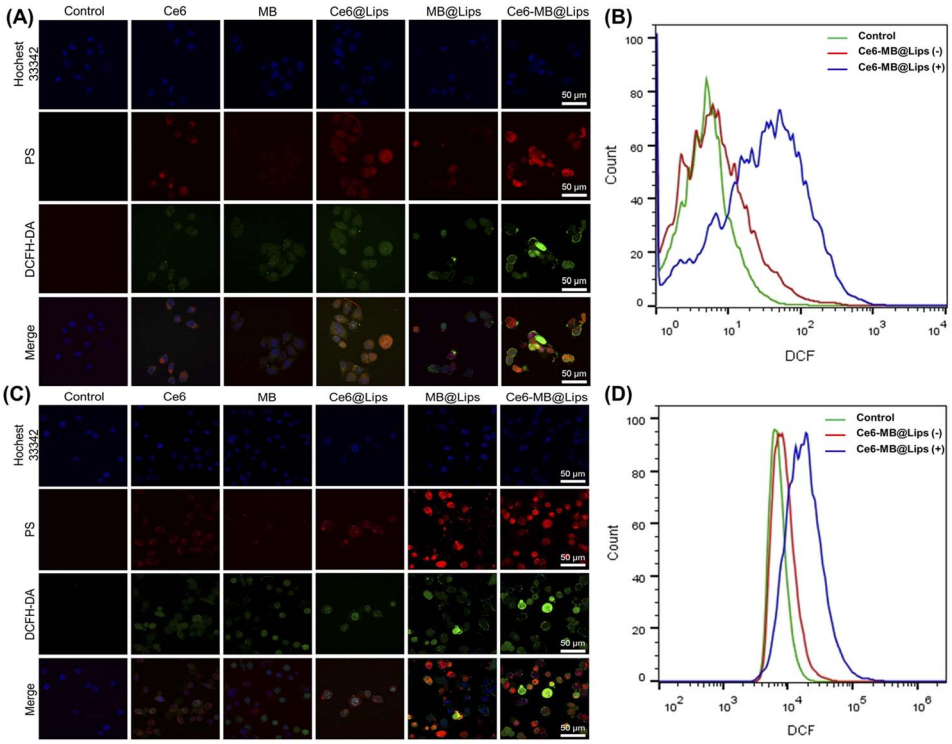

Fig. 5 ROS generation capacity. (A) CLSM fluorescence images of DCFH-DA-stained HeLa cells treated with Ce6, MB, Ce6@Lips, MB@Lips and Ce6-MB@Lips (scale bar: 50 μm, $\lambda_{ex} = 488$ nm, $\lambda_{em} = 525$ nm). (B) Shift in fluorescence peak due to the ROS generation in HeLa cells in the presence of Ce6-MB@Lips before irradiation (Ce6-MB@Lips (−)) and after irradiation (Ce6-MB@Lips (+)) with a 660 nm laser. (C) CLSM fluorescence images of DCFH-DA-stained SiHa cells treated with Ce6, MB, Ce6@Lips, MB@Lips and Ce6-MB@Lips (scale bar: 50 μm, $\lambda_{ex} = 488$ nm, $\lambda_{em} = 525$ nm). (D) Shift in fluorescence peak due to the ROS generation in SiHa cells in the presence of Ce6-MB@Lips before irradiation (Ce6-MB@Lips (−)) and after irradiation (Ce6-MB@Lips (+)) with a 660 nm laser.

comparison, the ROS production capacity of Ce6@Lips and MB@Lips was enhanced. As expected, the fluorescence signal of the Ce6-MB@Lips groups showed the most significant improvement after laser irritation, indicating more significant ROS production. To better verify the experimental phenomenon, we selected SiHa cells for the same treatment and detection. As shown in Fig. 5C, Ce6-MB@Lips also produced more ROS in SiHa cells, as in HeLa cells, indicating the excellent ability of Ce6-MB@Lips to generate ROS *in vitro*.

The amount of ROS produced in HeLa and SiHa cells was quantitatively assessed by a flow cytometer to support the PDT efficacy of Ce6-MB@Lips. As shown in Fig. 5B and D, after a 660 nm laser irradiation, the fluorescence peaks shifted to the right because of the regeneration of the ROS, indicating that

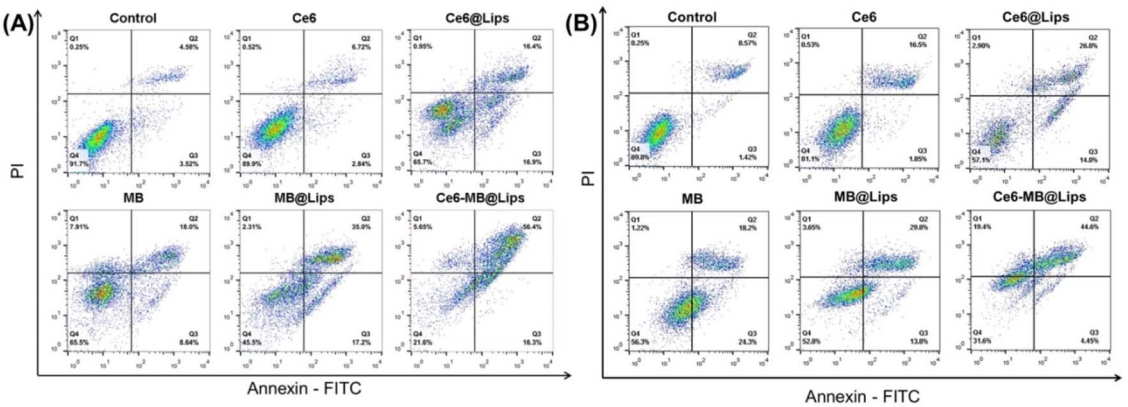

Fig. 6 Flow cytometer analysis of the apoptosis and necrosis of (A) HeLa cells, and (B) SiHa cells treated with PBS, Ce6, Ce6@Lips, MB, MB@Lips, Ce6-MB@Lips in the presence of laser irradiation (660 nm, 1 W cm^{-2}, 5 min) (Q1: necrotic cells; Q2: late apoptotic cells; Q3: early apoptotic cells; Q4: live cells).

Open Access Article. Published on 24 January 2023. Downloaded on 2/25/2026 2:49:08 PM. This article is licensed under a Creative Commons Attribution-NonCommercial 3.0 Unported Licence.

660 nm laser caused Ce6-MB@Lips generate more ROS in HeLa and SiHa cells.

Apoptotic analysis

To further confirm the phototoxicity of Ce6-MB@Lips, Annexin-V-FITC/PI double staining method was used to detect the apoptosis and necrosis of HeLa and SiHa cells. As shown in Fig. 6, under the same irradiation condition (660 nm, 1 W cm^{-2}, 5 min), the HeLa cell death rate of the Ce6-MB@Lips group was measured to be 78.35% (apoptosis rate was 72.7%, necrosis rate was 5.65%), which was significantly higher than that of free Ce6 group (10.08%), free MB group (34.55%), Ce6@Lips group (34.25%) and MB@Lips group (54.51%). To further verify the experimental phenomenon, the apoptosis of SiHa cells under identical treatment conditions was evaluated. The SiHa cell death rate of the Ce6-MB@Lips group was 68.45% (apoptosis rate was 49.05%, necrosis rate was 19.4%), which was significantly higher than that of the free Ce6 group (18.88%), free MB group (43.72%), Ce6@Lips group (42.9%) and MB@Lips group (47.25%). Therefore, Ce6-MB@Lips has the high phototoxicity to HeLa and SiHa cells, showing its application prospect in cervical tumor therapy.

Conclusion

In summary, we have successfully prepared a novel type of PS Ce6-MB@Lips which can be excited by a NIR-I laser at 660 nm. As expected, Ce6-MB@Lips had good stability, water solubility, and $^1O_2$-generation capacity. The results of *in vitro* experiments suggested that Ce6-MB@Lips showed lower toxicity to normal cells than to tumor cells. Ce6-MB@Lips showed high cell uptake efficiency, well phototoxicity, and a strong ability to produce ROS. The *in vitro* PDT effect was then evaluated by simultaneous application of nanoparticles and laser irradiation. The results showed that Ce6-MB@Lips produced a large number of ROS in the tumor cells to more effectively induce apoptosis of HeLa and SiHa cells, and the apoptosis rates were 78.35% and 68.45% respectively. Therefore, our work provides an innovative strategy, which is to induce PDT with a single NIR-I laser by coating two PSs with similar excitation wavelength with liposomes, to make more tumor cells apoptosis.

Author contributions

Nuernisha Alifu and Xueliang Zhang provided creativity and planning in the research. Gulinigaer Alimu performed a modification of nanoparticles guided by Nuernisha Alifu and Xueliang Zhang. Gulinigaer Alimu, Ting Yan, Lijun Zhu, and Zhong Du performed the *in vitro* works. Gulinigaer Alimu wrote the manuscript and Rong Ma, Huimin Fan and Shuang Chen contributed to the characterization of nanoparticles and editing of the manuscript. All authors have read and agreed to the published version of the manuscript.

Conflicts of interest

There are no conflicts to declare.

Acknowledgements

This work was supported by the Xinjiang Uygur Autonomous Region Regional Collaborative Innovation Special Science and Technology Assistance Program (2022E02130), the National Natural Science Foundation of China (NSFC) under Grant (Program No. 62035011 and No. 82060326), Xinjiang Medical University/State Key Laboratory of Pathogenesis, Prevention and Treatment of High Incidence Diseases in Central cultivation project of National Science Foundation for outstanding young people (xyd2021Y005), State Key Laboratory of Pathogenesis, Prevention and treatment of High Incident Diseases in central Asia (SKL-HIDCA-2022-3).

Notes and references

1 M. S. Lopez, E. S. Baker, M. Maza, G. Fontes-Cintra, A. Lopez, J. M. Carvajal, F. Nozar, V. Fiol and K. M. Schmeler, *J. Surg. Oncol.*, 2017, **115**, 615–618.
2 W. Small Jr, M. A. Bacon, A. Bajaj, L. T. Chuang, B. J. Fisher, M. M. Harkenrider, A. Jhingran, H. C. Kitchener, L. R. Mileshkin, A. N. Viswanathan and D. K. Gaffney, *Cancer*, 2017, **123**, 2404–2412.
3 U. Pandey and P. Bansel, *J. Gynecol. Women's Health*, 2017, **2**, 555599.
4 Z. Hu and D. Ma, *Cancer Med.*, 2018, **7**, 5217–5236.
5 C. Schlosser, N. Bodenschatz, S. Lam, M. Lee, J. N. McAlpine, D. M. Miller, D. J. Van Niekerk, M. Follen, M. Guillaud, C. E. MacAulay and P. M. Lane, *J. Biomed. Opt.*, 2016, **21**, 126011.
6 S. P. Mathur, R. S. Mathur, W. T. Creasman, P. B. Underwood and M. Kohler, *Cancer Biomarkers*, 2005, **1**, 183–191.
7 R. G. Ghebre, S. Grover, M. J. Xu, L. T. Chuang and H. Simonds, *Gynecol. Oncol. Rep.*, 2017, **21**, 101–108.
8 Z. Li, Y. Zhang, S. Sui, Y. Hua, A. Zhao, X. Tian, R. Wang, W. Guo, W. Yu, K. Zou, W. Deng, L. He and L. Zou, *J. Exp. Clin. Cancer Res.*, 2020, **39**, 243.
9 L. Chen, W. N. Zhang, S. M. Zhang, Z. H. Yang and P. Zhang, *Asian Pac. J. Cancer Prev.*, 2014, **15**, 10971–10975.
10 Y. Xiong, Z. Xu and Z. Li, *Front. Chem.*, 2019, **7**, 471.
11 M. Lismont, L. Dreesen and S. Wuttke, *Adv. Funct. Mater.*, 2017, **27**, 1606314.
12 L. R. Carobeli, L. E. F. Meirelles, G. Damke, E. Damke, M. V. F. Souza, N. L. Mari, K. H. Mashiba, C. S. Shinobu-Mesquita, R. P. Souza, V. Silva, R. S. Goncalves, W. Caetano and M. E. L. Consolaro, *Pharmaceutics*, 2021, **13**, 2057.
13 A. Bienia, O. Wiechec-Cudak, A. A. Murzyn and M. Krzykawska-Serda, *Pharmaceutics*, 2021, **13**, 1147.
14 Y. Liu, J. Tian, Y. Fu, Y. Yang, M. Chen and Q. Zhang, *Biomater. Sci.*, 2021, **9**, 700–711.
15 D. H. Li, L. Li, P. X. Li and X. Y. Chen, *OncoTargets Ther.*, 2015, **8**, 703–711.

© 2023 The Author(s). Published by the Royal Society of Chemistry

Open Access Article. Published on 24 January 2023. Downloaded on 2/25/2026 2:49:08 PM. This article is licensed under a Creative Commons Attribution-NonCommercial 3.0 Unported Licence.

16 D. van Straten, V. Mashayekhi, H. S. de Bruijn, S. Oliveira and D. J. Robinson, *Cancers*, 2017, **9**, 19.
17 Z. Youssef, R. Vanderesse, L. Colombeau, F. Baros, T. Roques-Carmes, C. Frochot, H. Wahab, J. Toufaily, T. Hamieh, S. Acherar and A. M. Gazzali, *Cancer Nanotechnol.*, 2017, **8**, 6.
18 S. H. Hong and Y. Choi, *J. Pharm. Invest.*, 2018, **48**, 3–17.
19 J. Qian, N. Alifu, X. Dong, D. Li, X. Sun, A. Zebibula, D. Zhang and G. Zhang, *Mater. Chem. Front.*, 2017, **1**, 1746–1753.
20 X. Zhuang, X. Ma, X. Xue, Q. Jiang, L. Song, L. Dai, C. Zhang, S. Jin, K. Yang, B. Ding, P. C. Wang and X. J. Liang, *ACS Nano*, 2016, **10**, 3486–3495.
21 S. R. Lee and Y. J. Kim, *Nanomaterials*, 2018, **8**, 445.
22 X. S. Li, D. Y. Lee, J. D. Huang and J. Y. Yoon, *Angew. Chem.*, 2018, **57**, 9885–9890.
23 J. M. Chen, T. J. Fan, Z. J. Xie, Q. Q. Zeng, P. Xue, T. T. Zheng, Y. Chen, X. L. Luo and H. Zhang, *Biomaterials*, 2020, **237**, 119827.
24 D. K. Chatterjee, S. F. Li and Y. Zhang, *Adv. Drug Delivery Rev.*, 2008, **60**, 1627–1637.
25 Y. Zhu, C. Chen, Z. Cao, S. Shen, L. Li, D. Li, J. Wang and X. Yang, *Theranostics*, 2019, **9**, 8312–8320.
26 R. Vankayala and K. C. Hwang, *Adv. Mater.*, 2018, **23**, 1706320.
27 Y. Sun, C. Qu, H. Chen, M. He, C. Tang, K. Shou, S. Hong, M. Yang, Y. Jiang, B. Ding, Y. Xiao, L. Xing, X. Hong and Z. Cheng, *Chem. Sci.*, 2016, **7**, 6203–6207.
28 M. G. Adimoolam, A. Vijayalakshmi, M. R. Nalam and M. V. Sunkara, *J. Mater. Chem. B*, 2017, **5**, 9189–9196.
29 D. H. Kang, H. M. Lee, C. W. Chung, C. H. Kim, D. H. Kim, T. W. Kwak and Y. I. Jeong, *Drug Des., Dev. Ther.*, 2014, **8**, 1451–1462.
30 Y. X. Zhu, H. R. Jia, Z. Chen and F. G. Wu, *Nanoscale*, 2017, **9**, 12874–12884.
31 C. Feng, L. Chen, Y. Lu, J. Liu, S. Liang, Y. Lin, Y. Li and C. Dong, *Front. Chem.*, 2019, **7**, 853.
32 H. Zhang, W. Li, G. Tan, G. Ding, Z. Wang and Y. Jin, *RSC Adv.*, 2017, **7**, 40873–40880.
33 Y. Shen, T. Wu, Y. Wang, S. L. Zhang, X. Zhao, H. Y. Chen and J. J. Xu, *Anal. Chem.*, 2021, **93**, 4042–4050.
34 Y. Wan, G. H. Lu, W. C. Wei, Y. H. Huang and C. S. Lee, *ACS Nano*, 2020, **8**, 9917–9928.
35 D. J. Lim, *Polymers*, 2021, **13**, 3955.
36 A. F. Dos Santos, L. F. Terra, R. A. Wailemann, T. C. Oliveira, V. M. Gomes, M. F. Mineiro, F. C. Meotti, A. Bruni-Cardoso, M. S. Baptista and L. Labriola, *BMC Cancer*, 2017, **17**, 194.
37 L. Yu, Z. Wang, Z. Mo, B. Zou and Z. Yu, *Acta Pharm. Sin. B*, 2021, **11**, 2004–2015.
38 G. K. Park, J. H. Lee, E. Soriano, M. Choi, K. Bao, W. Katagiri, D. Y. Kim, J. H. Paik, S. H. Yun, J. V. Frangioni, T. E. Clancy, S. Kashiwagi, M. Henary and H. S. Choi, *iScience*, 2020, **23**, 101006.
39 R. Nisini, N. Poerio, S. Mariotti, F. D. Santis and M. Fraziano, *Front. Immunol.*, 2018, **9**, 155.
40 P. Skupin-Mrugalska, J. Piskorz, T. Goslinski, J. Mielcarek, K. Konopka and N. Duzgunes, *Drug Discovery Today*, 2013, **18**, 776–784.
41 P. Yingchoncharoen, D. S. Kalinowski and D. R. Richardson, *Pharmacol. Rev.*, 2016, **68**, 701–787.
42 H. Abrahamse, C. A. Kruger, S. Kadanyo and A. Mishra, *Photomed. Laser Surg.*, 2017, **35**, 581–588.
43 W. Lee and H. J. Im, *Nucl. Med. Mol. Imaging*, 2019, **53**, 242–246.
44 K. Zhang, Y. Zhang, X. Meng, H. Lu, H. Chang, H. Dong and X. Zhang, *Biomaterials*, 2018, **185**, 301–309.
45 B. Li, Z. Meng, Q. Li, X. Huang, Z. Kang, H. Dong, J. Chen, J. Sun, Y. Dong, J. Li, X. Jia, J. L. Sessler, Q. Meng and C. Li, *Chem. Sci.*, 2017, **8**, 4458–4464.
46 Y. Mohammed, A. J. Percy, A. G. Chambers and C. H. Borchers, *J. Proteome Res.*, 2015, **14**, 1137–1146.
47 T. Yan, G. Alimu, L. Zhu, H. Fan, L. Zhang, Z. Du, R. Ma, S. Chen, N. Alifu and X. Zhang, *ACS Omega*, 2021, **7**, 44643–44656.
48 L. Lin, H. Lin, Y. Shen, D. Chen, Y. Gu, B. C. Wilson and B. Li, *Photochem. Photobiol.*, 2020, **96**, 646–651.
49 A. Campu, M. Focsan, F. Lerouge, R. Borlan, L. Tie, D. Rugina and S. Astilean, *Colloids Surf., B*, 2020, **194**, 111213.
50 L. Duan, L. Wang, C. Zhang, L. Yu, F. Guo, Z. Sun, Y. Xu and F. Yan, *Int. J. Clin. Exp. Pathol.*, 2019, **12**, 2353–2362.
51 Y. Xia, T. Xu, C. Wang, Y. Li, Z. Lin, M. Zhao and B. Zhu, *Int. J. Nanomed.*, 2018, **13**, 143–159.
52 H. Pan, H. Shi, P. Fu, P. Shi and J. Yang, *ACS Omega*, 2021, **6**, 3991–3998.
53 Q. L. Ma, M. O. Shen, N. Han, H. Z. Xu, X. C. Peng, Q. R. Li, T. T. Yu, L. G. Li, X. Xiang, B. Liu, X. Chen, M. F. Wang and T. F. Li, *Photodiagn. Photodyn. Ther.*, 2022, **37**, 102645.
54 J. Chen, Y. Zhang, Z. Meng, L. Guo, X. Yuan, Y. Zhang, Y. Chai, J. L. Sessler, Q. Meng and C. Li, *Chem. Sci.*, 2020, **11**, 6275–6282.
55 Z. Z. Li, D. Wang, M. S. Xu, J. M. Wang, X. L. Hu, S. Anwar, A. Claudiotedesco, P. Cesarmorais and H. Bi, *J. Mater. Chem. B*, 2020, **8**, 2598–2606.
56 J. Liang, P. Wu, C. Tan and Y. Jiang, *RSC Adv.*, 2018, **8**, 9218–9222.
57 Y. Yang, H. Liu, P. Han, B. Sun and P. Li, *Angew. Chem., Int. Ed.*, 2016, **55**, 13538–13543.
58 D. Yu, Y. Zha, Z. Zhong, Y. Ruan and S. Hou, *Sens. Actuators B Chem.*, 2021, **339**, 129878.

© 2023 The Author(s). Published by the Royal Society of Chemistry